Available online at www.sciencedirect.com

SciVerse ScienceDirect

Ceramics International 39 (2013) 4791–4799

CERAMICS INTERNATIONAL

www.elsevier.com/locate/ceramint

Sintering mechanisms of Yttria with different additives

X. Cheng[a,*], C. Yuan[a], N.R. Green[a], P.A. Withey[a,b]

[a]School of Metallurgy and Materials, University of Birmingham, Birmingham B15 2TT, UK
[b]Rolls-Royce plc, P.O. Box 31, Derby DE24 8BJ, UK

Received 30 April 2012; received in revised form 21 November 2012; accepted 22 November 2012
Available online 1 December 2012

Abstract

The sintering behaviour of conventional yttria powder was investigated, with emphasis on the effect of sintering additives such as B_2O_3, YF_3, Al_2O_3, ZrO_2, and TiO_2, etc. at sintering temperatures from 1000 °C to 1600 °C. Powder shrinkage behaviour was analysed using a dilatometer. The powder sintering mechanisms were identified at different temperatures using powder isothermal shrinkage curves. This analysis showed that the sintering additives B_2O_3 and YF_3 could improve yttria sintering by changing the diffusion/sintering mechanisms at certain temperatures, while sintering additives TiO_2, Al_2O_3 and ZrO_2 appeared to retard the powder densification at temperatures around 1000 °C and are more suitable when used at temperatures in excess of 1300 °C. The powder with La_2O_3 added had the slowest densification rate throughout the test temperatures in this experiment and was also found to be more suitable when used at temperatures higher than 1550 °C.

Keywords: A. Sintering; C. Thermal expansion; D. Y_2O_3; E. Structural application

1. Introduction

Yttrium oxide (Y_2O_3) has excellent inertness, refractory character, high melting temperature (2410 °C) and optical properties, and has now become a very attractive material for industrial applications [1,2]. Because of its superior inertness to chemical attack from molten Ti alloys during investment casting, yttria has been widely used as a face-coat material in the investment casting of titanium aluminide alloys for a number of years [3–5]. As a rare earth material, yttria requires a very high sintering temperature, in excess of 1700 °C, in order to achieve a high density [6]. However, high sintering temperatures ($\geq$ 1400 °C) for an yttria face-coat will add to the production cost of the moulds. But reducing the sintering temperature will lead to poorly-bonded yttria particles on the finished mould surface. These loose particles will be easily pulled out during casting and will remain in the metal after solidification, becoming inclusions [7]. Meanwhile, the uneven mould surface will also affect the surface finish of the final components.

In order to enhance the sintering properties of yttria face-coats at relatively low temperatures, additives such as ZrO_2 [8], ThO_2 [9], Al_2O_3 [10,11], La_2O_3 [12], CaO [13], MgO [13], and B_2O_3 [14] were studied. These sintering additives can enhance yttria sintering by changing sintering mechanisms. Some of them can react with yttria to form new transient liquid phases at comparatively low temperatures and enhance yttria powder sintering. In this work, new sintering additive compounds such as YF_3, and TiO_2 are also investigated.

Powder sintering behaviour has been investigated by many researchers [15–20,22], and several methods have been published to identify the sintering mechanisms after introducing different sintering additives. Johnson and Cutler [19], and Matsui [18] reported that the sintering mechanical numerical constant '*n*' can be predicted by studying the isothermal shrinkage behaviour of the compacts. Wang [21] applied these methods to predict the sintering mechanisms and activation energy of sintering pure yttria, and the results show that by sintering at around 1400 °C, yttria suffers grain-boundary diffusion with activation energy of around 410 kJ/mol. Sintering additions of Mg and Nb can influence the yttria sintering rate by changing the activation energy.

The current research was carried out to study the shrinkage behaviour of yttria after adding sintering additives

*Corresponding author. Tel.: +44 121 4147839; fax: +44 121 4147890.
E-mail address: chengxu87@hotmail.com (X. Cheng).

0272-8842/$ - see front matter © 2012 Elsevier Ltd and Techna Group S.r.l. All rights reserved.
http://dx.doi.org/10.1016/j.ceramint.2012.11.069

including B_2O_3, YF_3, TiO_2, Al_2O_3, and La_2O_3 to enhance powder sintering at temperatures of around 1000 to 1600 °C. In this study, the sintering mechanisms (n) of each sintering additive were analysed based on isothermal heating dilatometer methods. Powder particle morphologies at different sintering temperatures were observed using scanning electron microscopy (SEM), and the powder compositions at different temperatures were identified by X-ray diffraction (XRD).

2. Materials and methods

Yttria powder with a mean particle size of 14 μm (−200 mesh, Treibacher Industrie AG) was used as the starting powder and blended with the sintering additives listed in Table 1. Powders with additives were first mixed in de-ionised water overnight and dried. About 3 g of dried powder was weighed and pressed to a cylindrical compact (13 mm in diameter) under a constant pressure of 26 MPa using an Instron™ mechanical testing machine.

The particle size distributions of the various fillers were analysed using laser powder particle size measuring equipment (Coulter LS230), and the microstructure evolution of the powder compact was analysed using a scanning electron microscope after sintering at four different temperatures, 1000, 1200, 1400 and 1600 °C for 1 h in air. The anisotropic shrinkage of the compacts during heating was measured as a function of time using a dilatometer (NETZSCH DIL 402E). The compacts were heated at a rate of 20 °C/min to the different isothermal temperatures, namely 1000 °C, 1200 °C, 1300 °C and 1550 °C, held at temperature for 1 h and then cooled down at the same rate to room temperature in air. The phase transformations during the heating and dwelling process at each temperature range were identified using X-Ray diffraction with a beam incident angle between 20° and 100°.

3. Theory and calculation

3.1. Isothermal shrinkage

The sintering-rate equation for isothermal shrinkage at the initial sintering stage is given by Eq. (1) [19]:

$$\left(\frac{\Delta L}{L_0}\right) = \left(\frac{K\gamma\Omega D}{kTa^p}\right)^n t^n \quad (1)$$

where:

$\Delta L/L_0$ = fraction shrinkage, L_0 is the sample original length, and ΔL is the length change.
T = absolute temperature,
K = numerical constant,
D = self-diffusion coefficient,
γ = surface energy,
t = time,
k = Boltzmann's constant,
a = the spherical particle radius
n, p = sintering indices, themselves dependent on the diffusion mechanisms [22] and
Ω = atomic volume.

On taking logarithms, Eq. (2) is obtained:

$$\log\left(\frac{\Delta L}{L_0}\right) = n\log\left(\frac{K\gamma\Omega D}{kTa^p}\right) + n\log t \quad (2)$$

As, for certain sintering mechanisms and temperatures, $n\log(K\Omega\gamma D/kTa^p)$ equals to a constant A, the Eq. (2) can be written as: $\log(\Delta L/L_0) = A + n\log(t)$. Plotting $\log(\Delta L/L_0)$ against $\log(t)$, the mechanism specific constant n can be obtained. Johnson and Cutler [19,23] reported that the difficulty of measurement of the powder compact dimension change of isothermal sintering due to experimental errors caused by powder pre-sintering before reaching the set isothermal holding temperature. In order to minimise the pre-sintered problems of powder during heating, Matsui [18] applied a corrective factor δL in Eq. (2) with the correction time t_0 to analyse the sintering properties of ZrO_2 powder with small amounts of Y_2O_3 additives. Based on Matsui's research, a new method was developed and used in this research to predict powder sintering mechanisms at the early stage of sintering. This new method used a corrected length $\Delta L_{(cor)}$ to replace ΔL and a corrected isothermal sintering time $(t - t_o)$ to replace t in Eq. (2). The definition of each factor is illustrated in Fig. 1.

4. Results and discussion

4.1. Raw powder particle-size distribution and microstructure

The powder particle-size distribution before test is given in Fig. 2(a). It can be seen that the sintering additives had a

Table 1
sintering powder compositions.

Sample ID	Additives	wt% of pure element	mol% of sintering additives
Sample Y	As received pure yttria −200 mesh powder		
Sample YB	B_2O_3	2.0	17.4
Sample YAZ	Al_2O_3, ZrO_2	0.5 wt%Al_2O_3–0.5 wt%ZrO_2 commercially available powder	
Sample YT	TiO_2	2.0	8.56
Sample YF	YF_3	2.0	7.43
Sample YLa	La_2O_3	2.0	1.57

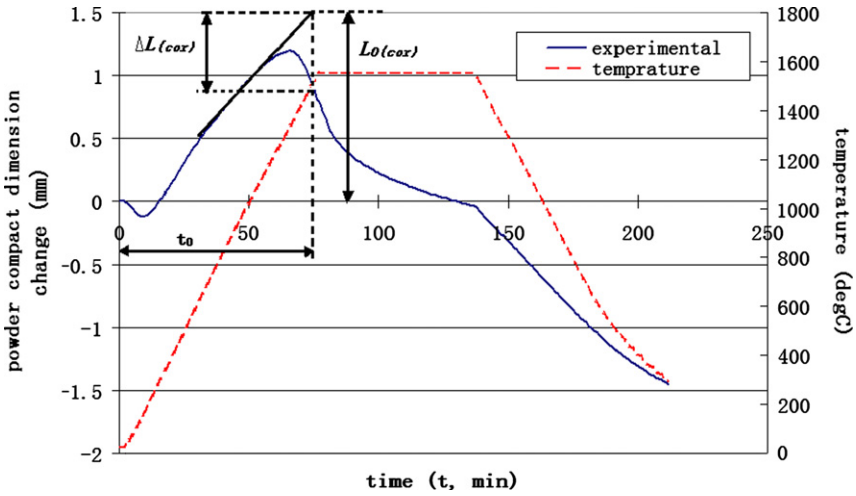

Fig. 1. A schematic diagram dilatometer test trace of the correction methods with annotations used in this paper.

narrower powder particle size distribution when compared to pure yttria. This might be due to particle agglomeration, and which could be caused by the electrical charge at the powder surface after adding the additives. The microstructure of the pure −200 mesh yttria is shown in Fig. 2(b).

4.1.1. Powder XRD

Phase transformation of sample powders at different sintering temperatures of 1000, 1200, 1400, and 1600 °C were examined by XRD and the results are shown in Fig. 3.

As can be seen from Fig. 3(a), very weak YF_3 peaks were detected in sample YF when sintered at a temperature of 1000 °C. By increasing the temperature to around 1200 °C, YF_3 phase peaks disappeared and only yttria peaks were detected. This observation results confirmed with Russel [24] and Mosiadz [25] observation, that the compound YF_3 has a stabilisation temperature of around 900 °C and high temperature sintering will cause YF_3 to evaporate and hardly be detected.

Compared to the YF_3 system, adding TiO_2 into yttria caused a very complicated phase transformation to take place. At the sintering temperature of around 1000 °C, TiO_2 first reacted with yttria to form a Y_2TiO_5 phase, and this phase gradually transformed into a YTiO phase at a temperature around 1400 °C. Kim et al. [26] reported that this Y_2TiO_5 phase was formed at a temperature around 920 °C, and at high temperatures, around 1390 °C, the Y_2TiO_5 phase transformed into a fluorite type structure [27,28].

Boron can interact with yttria to form different compounds at different temperatures [29]. At about 1000 °C, B_2O_3 is interacted with yttria to form an YBO_3 phase, and later another yttrium borate phase, Y_3BO_6, at a temperature of around 1200 °C was formed. The phase transformations observed in this experiment were confirmed with the literatures [30–33].

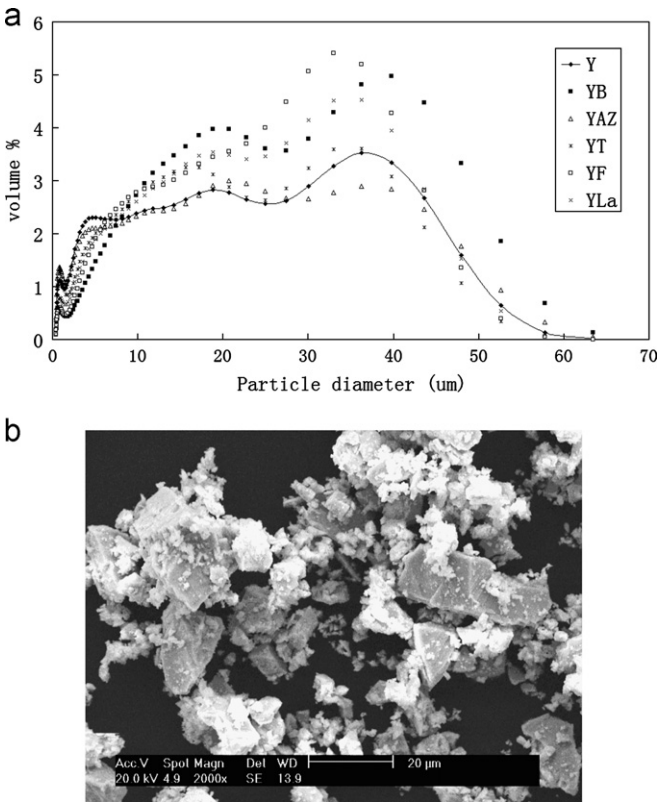

Fig. 2. (a) The powder particle size distribution of the different test samples, and (b) the microstructure of as received −200 mesh yttria powder.

Unfortunately, for sample YAZ, only yttria peaks were detected at all sintering temperatures. From the literature [34–37], small amounts of ZrO_2 and Al_2O_3 can form a solid solution in yttria with no detectable peak change. Another reason for little change may be that the amount of the additives of ZrO_2 and Al_2O_3 was too low in this commercially available powder and below the sensitivity of the XRD test. Besides YAZ powder, there were also no new

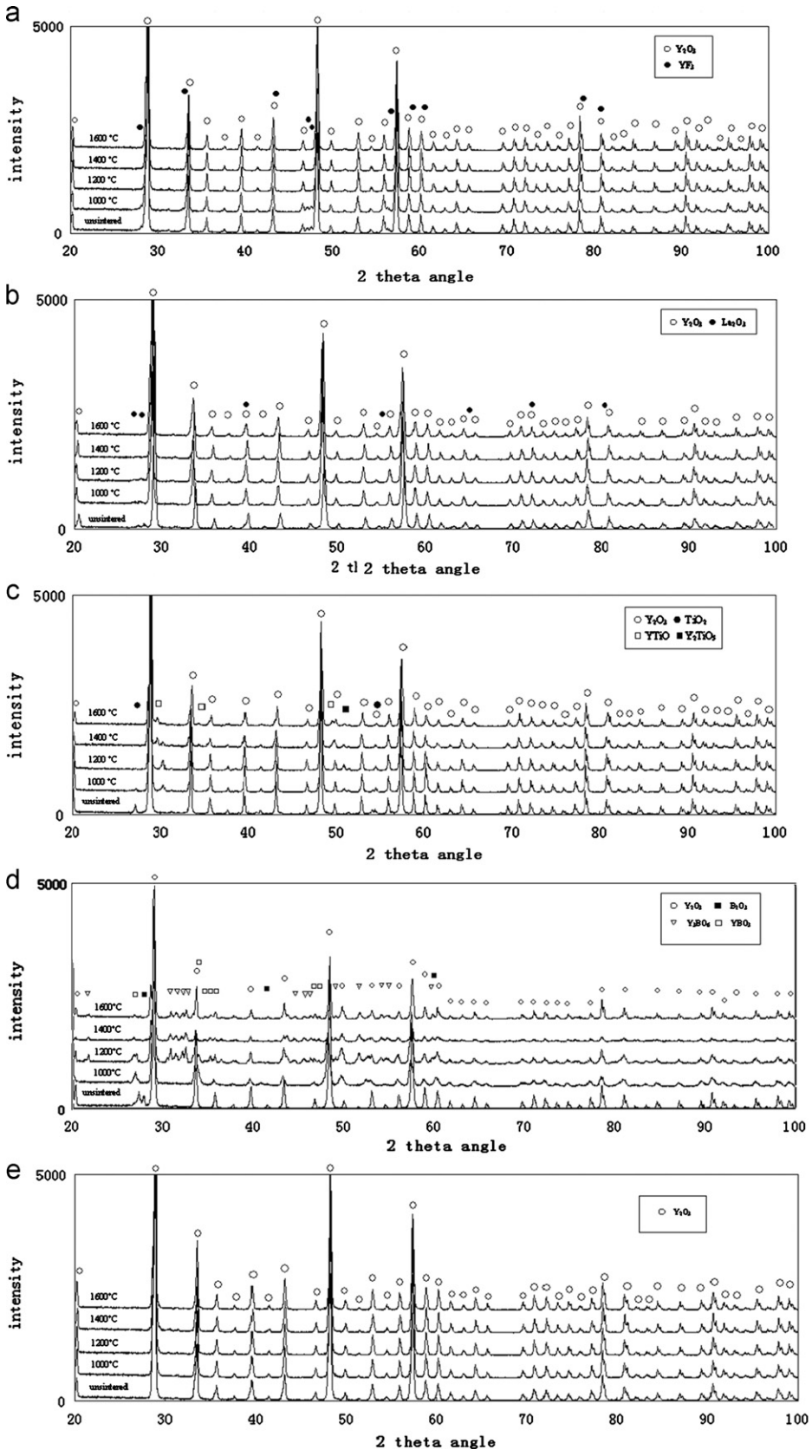

Fig. 3. XRD test results of powders sintered at different temperatures, (a) YF, (b) YLa, (c)YT, (d)YB, and (e) YAZ.

compound peaks found throughout all the testing temperatures of the sample containing 2.0 wt% La_2O_3. This may be explained by the sintering additive La_2O_3 having very wide solubility in yttria from 0 to 20 mol% [38], so it becomes a solid solute in the yttria lattice and hardly detected.

4.1.2. Powder compact microstructure change

The powder compact microstructure is different for different sintering additives systems and temperatures. By observing powder-particle microstructures at different temperatures (Fig. 4), it can be seen that the first observed change is the shape of particles changing from angular to smooth. Then, at higher sintering temperatures, more materials diffused and this caused the formation of networks between particles. However, for some sample powders (e.g. YB), upon reaching a certain temperature, mass flow or diffusion took place with the dissolution of small particles and the subsequent growth of large particles to form new large spherical grains with pores trapped at the grain boundaries.

4.1.3. Powder isothermal shrinkage properties

Powder compact isothermal heating properties were measured using the dilatometer at different temperatures, see Fig. 5.

As can be seen, after sintering at different temperatures, the powder sintering behaviour is different for different sintering additives. Due to low temperature dilatometer 'bedding in', there is a small amount of shrinkage taking place in every sample at the temperatures around 200 °C. After each sintering cycle, the total powder shrinkage is different depending on the additive, e.g. for the yttria powder sintered at around 1550 °C, the total $(dL/L_0)\%$ shrinkage which took place is around 1.2% (Fig. 5(a)). The magnitude of the total shrinkage of the powder compact is dependent on the sintering temperature and type of sintering additives, and the total shrinkage for each sample after the different heating cycles shown in Fig. 5 is listed in Table 2 below.

As is illustrated in Table 2, the higher sintering temperatures lead to larger shrinkage taking place. Compared with the pure yttria compact, some powders with additives seem to enhance the powder densification at temperatures around 1200 °C, especially the YB and YF powder systems. As the sintering temperature reached to 1300 °C, the samples YF, YB and YT showed very obvious shrinkage, and the YLa sample had the smallest shrinkage at around 0.17% which was even smaller than that for pure yttria at around 0.6%. The sintering behaviour of YAZ powder at 1300 °C is quite similar to that of the yttria powder. After sintering at 1550 °C for 1 h, except for the YLa sample, all the samples had a larger shrinkage than pure yttria. The slow densification of La doped yttria was also be observed by Huang et al. [40] in studying the sintering mechanism of 9 mol% lanthanum doped yttria who found that La ions can enhance grain-boundary mobility at temperatures from around 1500 °C to 1700 °C.

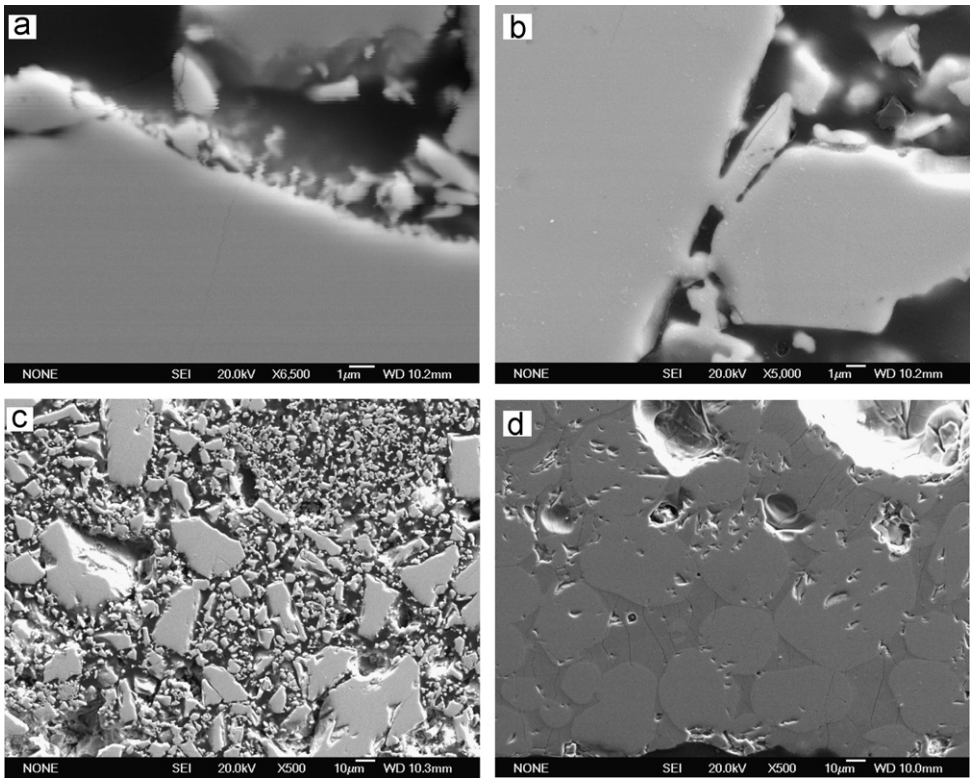

Fig. 4. YB sample powder microstructures at different sintering temperatures, (a) 1000 °C, (b) 1200 °C, (c) 1400 °C and (d) 1600 °C.

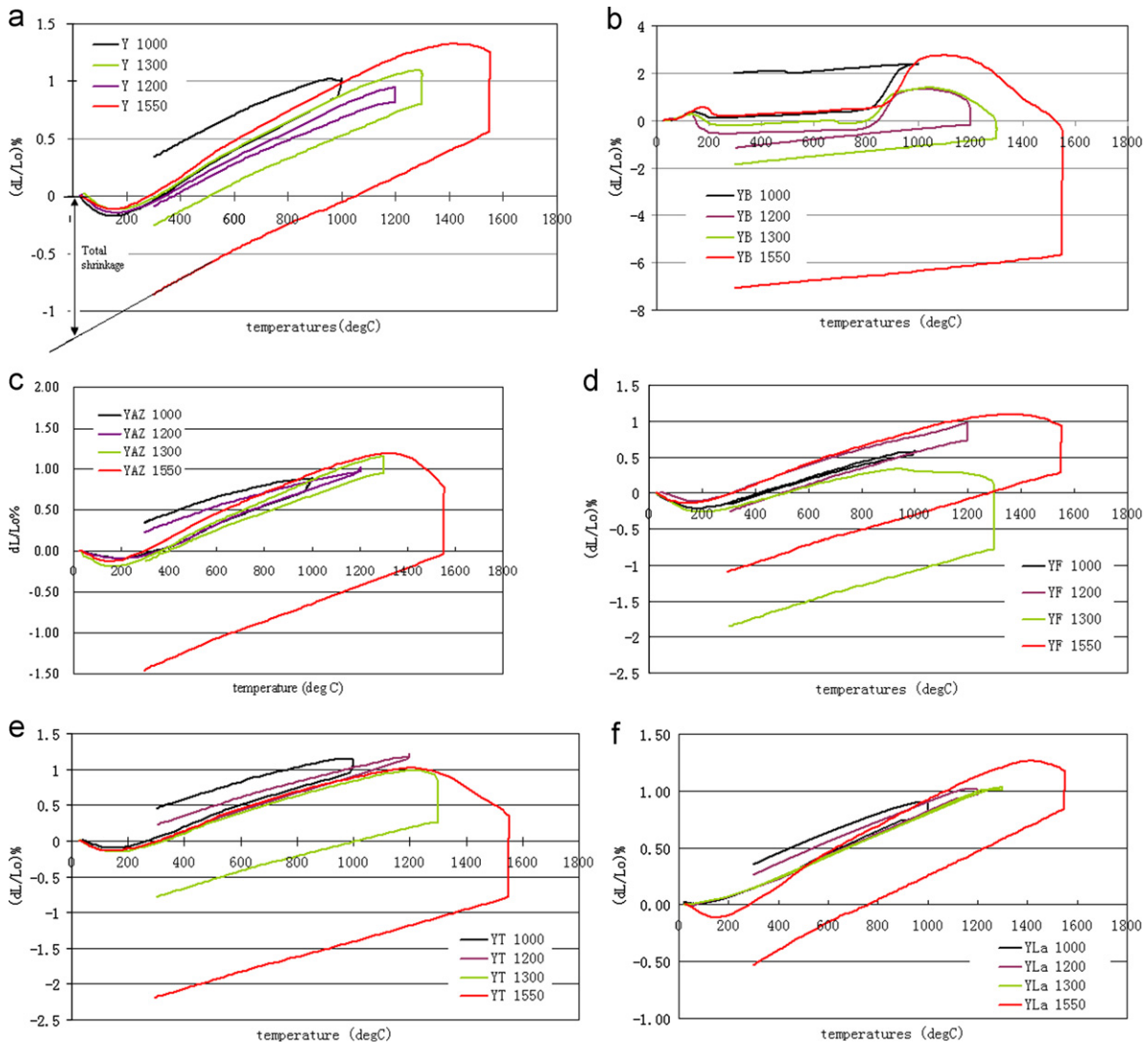

Fig. 5. The isothermal dilatometer trace of powders at different temperatures, (a)Y, (b) YB, (c)YAZ, (d)YF, (e) YT, and (f) YLa.

Table 2
The total shrinkages $(dL/L_0)\%$ of the samples for different heating cycles.

Sample	1000 °C	1200 °C	1300 °C	1550 °C
Y	**0**	**0.4**	**0.6**	**1.2**
YB	Expansion	1.2	2.2	7.3
YLa	0	0.05	0.17	0.85
YT	0	0.18	1.2	2.55
YF	0.45	0.5	2.25	1.5
YAZ	0	0.07	0.5	1.8

However, for samples YB and YAZ, there is an abnormal sample expansion taking place at temperatures around 1000 °C and 1200 °C, and these expansions may be due to an exothermic interaction which takes place between yttria and the sintering additives which causes the powder compact to expand.

After using the new correction method described in Section 3.1 of this paper, the corrected traces for isothermal sintering are shown in Fig. 6. This takes into consideration the pre-sintering of the powder during heating.

It can be seen that after the correction, the dimensional change of the powder compacts in the test direction increased with time. When sintering at 1000 °C, powders YT, YLa and YAZ expanded, and after the sintering temperature reached 1200 °C, all the powder compacts had started to sinter. High sintering temperatures caused larger densification to take place with higher sintering rates. During the isothermal sintering test, the powder YB showed the highest densification rate at all the test temperatures, and powder compacts with La_2O_3 and YAZ retarded the densification of the yttria.

By taking logarithms of $d(L_{cor}/L_{0cor})\%$ and $(t-t_0)$ using Eq. (2), the Arrhenius relationship of powder dimensional changes can be determined and is presented in Fig. 7 for

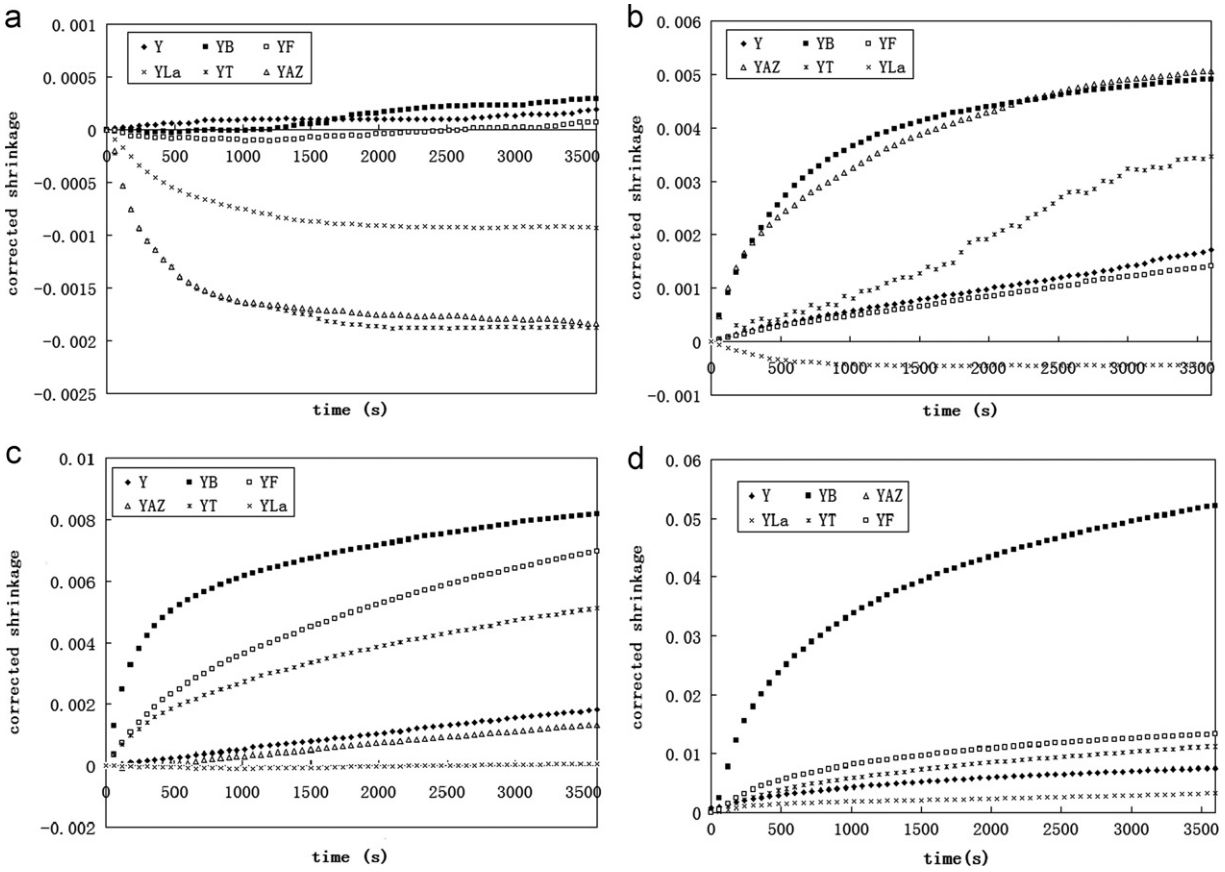

Fig. 6. The corrected shrinkage trace for the powder compacts during isothermal heating at temperatures of, (a) 1000 °C, (b) 1200 °C, (c) 1300 °C and (d) 1550 °C.

different isothermal shrinkage temperatures. (Because some powders expanded at lower temperatures, they are not used for this analysis).

When sintering at comparatively low temperature of 1000 °C, some of the powder dimensional change rates did not fully follow a linear relationship (YLa, YAZ and YT). The high sintering temperatures caused a more obvious densification of the powder compact and hence better matched the Arrhenius relationship. The mechanism-related numerical constant n can be obtained from the slope of the traces and is shown in Table 3.

According to Rahaman [39] and Lukin [41], the vapour diffusion sintering mechanism (VD) has an n value around 0.66, for bulk diffusion (BD) it is around 0.33–0.5, grain boundary (GBD) has n values around 0.25–0.31, while liquid-phase dissolution-precipitation (DP) mechanism have the smallest n value, of around 0.10. Therefore, from the above Table 3, it can be seen that at low sintering temperatures (e.g. around 1300 °C), the dominant sintering mechanism for yttria powder was bulk diffusion, and with increasing sintering temperature, the sintering mechanism gradually changed to grain boundary diffusion at temperatures around 1550 °C. Wang [21] suggested that the main sintering mechanism of yttria at temperatures from 1400 to 1500 °C is grain boundary diffusion, which very similar to this experimental prediction.

By adding sintering additives, the sintering mechanisms of powders were changed. Some additives such as B_2O_3 and YF_3 can enhance powder densification by changing the lattice diffusion of yttria to grain boundary diffusion at temperatures around 1200 °C, while the other additives such as La_2O_3 and TiO_2 retarded powder sintering and the densification only takes place at higher temperatures, which agreed with the results published by Huang [40] and Gasgnier [1] stating that the La^{3+} and Ti^{4+} ions can accelerate the grain growth of yttria, and the powder could start to densify at temperatures around 1500 °C and 1300 °C respectively.

However, this correction method suggested that at around 1200 °C, the dominant sintering mechanism of YB systems is liquid phase sintering. As it was know from the Y_2O_3–B_2O_3 phase diagram [29], the eutectic temperature is around 1373 °C, higher than the predicted liquid phase forming temperature. But the researches of Hu [42], Wu [43] and Luo [44] shows that the thin liquid pocket could form at the local area in the system at the temperature as much as 200 °C below the eutectic temperature due to the element segregation.

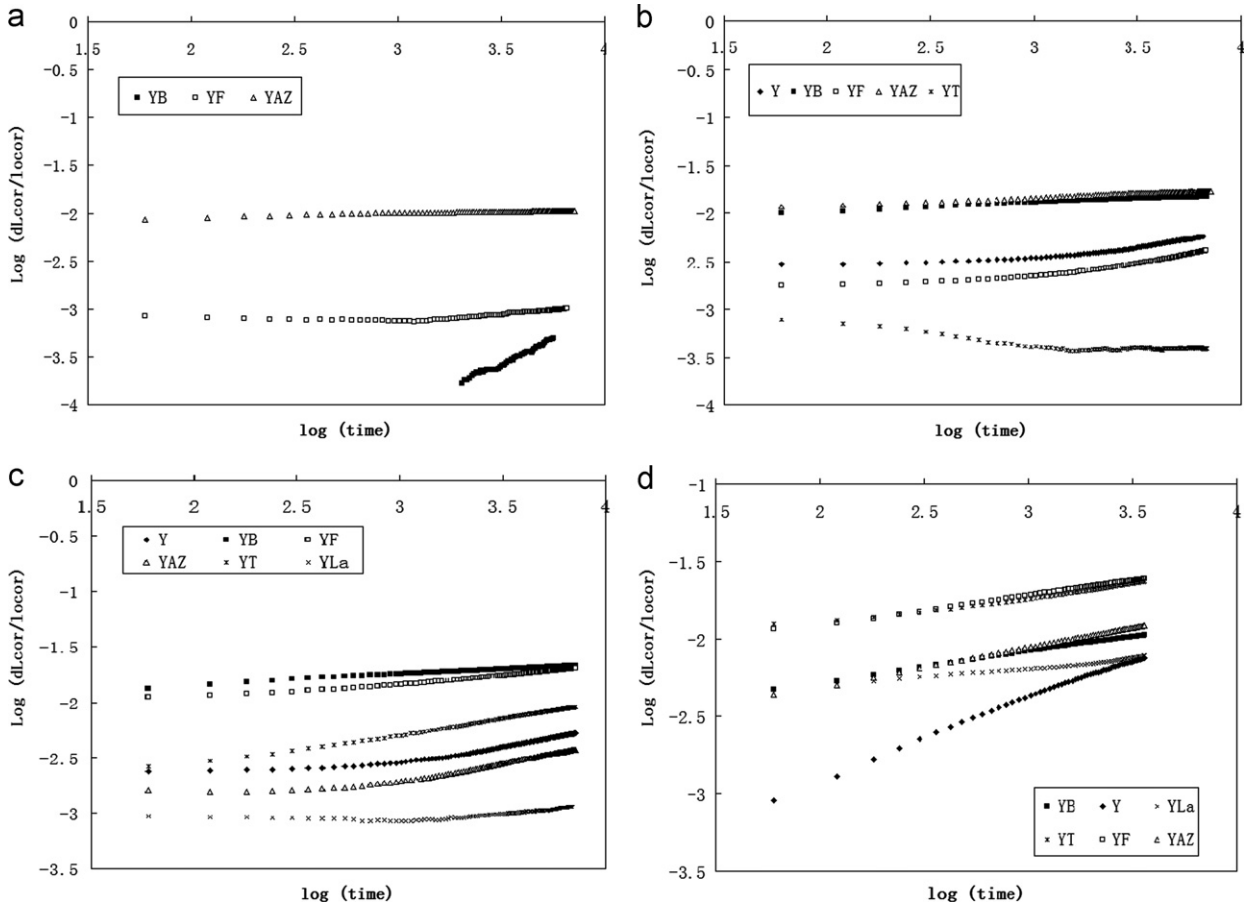

Fig. 7. The logarithms of the corrected shrinkage trace of powder during isothermal heating at different temperatures, (a) 1000 °C, (b) 1200 °C, (c) 1300 °C and (d) 1550 °C.

Table 3
Sintering mechanism '*n*' of each powder at different isothermal sintering temperatures.

Sample ID	1000 °C	1200 °C	1300 °C	1550 °C
Y	**Expansion**	**0.31**	**0.32**	**0.27**
YB	1.56	0.06	0.09	0.20
YAZ	Expansion	0.28	0.36	0.18
YF	0.19	0.34	0.18	0.19
YT	Expansion	2.86	0.27	0.21
YLa	Expansion	Expansion	0.17	0.16

5. Conclusions

In this study, different sintering additives were selected and added to yttria powder to enhance sintering properties in the initial stages of sintering. Based on this research there are some conclusions which can be drawn.

1. According to the isothermal shrinkage curves for the powder compacts, the sintering additives, B_2O_3 and YF_3 proved to be the most effective compounds in this study in promoting yttria sintering through enhancing materials diffusion enabling different sintering mechanisms at sintering temperatures from 1000 to 1600 °C.
2. Additives such as Al_2O_3, ZrO_2, and TiO_2 are more suitable for this application when the sintering temperature is higher than 1200 °C, and sintering additives such as La_2O_3 seemed to work only at temperatures exceeding 1550 °C.
3. The isothermal sintering-curve modification method used in this research showed a good correlation with the published data, except for the case when an exothermic interaction took place between yttria and the additives.

Acknowledgements

The authors would like to thank Rolls-Royce plc. for financial support to this programme and all the Research Fellows and Technicians in the Casting Group in the School of Metallurgy and Materials are gratefully acknowledged for their practical support.

References

[1] G. Gasgnier, J.F. Baumard, M. Boncoeur, M. Bougoin, Enhanced densification of yttria by addition of titanium oxide, Journal of the European Ceramic Society 13 (1994) 67–72.

[2] C. Greskovich, C.R. O'Clair, Transparent, sintered $Y_{2-x}Sr_x$, $O_{3-x/2}$ ceramics, Advanced Ceramic Materials 1 (1986) 350–355.
[3] C. Renjie, G. Ming, Z. Hu, G. Shengkai, Interactions between TiAl alloys and yttria refractory material in casting process, Journal of Materials Processing Technology 210 (2010) 1190–1196.
[4] E.S. Lassow, P.R. Johnson, Ceramic shell mould face coat and core coating systems for investment casting of reactive metals, USA, No. 4703806, November 1987.
[5] A. Horton Robert, Method of casting a reactive metal against a surface formed from an improved slurry containing yttria, US 4,947,927, August 1990.
[6] Y. Huang, D. Jiang, J. Zhang, Q. Lin, Fabrication of Transparent lanthanum-doped yttria ceramics by combination of two-step sintering and vacuum sintering, Journal of the American Ceramic Society 92 (2009) 2883–2887.
[7] Toshimitsu Tetsui, Toshiharu Kobayashi, Takashi Mori, Tatsuya Kishimoto, Hiroshi Harada, Evaluation of yttria applicability as a crucible for induction melting of TiAl alloy, Materials Transactions 51 (2010) 1656–1662.
[8] G.G. Bernard, Sinet Christophe, A sintered and doped yttrium oxide product, WO 2,007,107,954, December 2007.
[9] P.J. Jorgensen, R.C. Anderson, Grain-boundary segregation and final-stage sintering of Y_2O_3, Journal of the American Ceramic Society 50 (1967) 553–558.
[10] F. Joseph, Rhodes William H. Transparent yttria ceramics and method for producing same, US patent 4,166,831, September 1979.
[11] D. Hotza, A. Leo, J. Sunarso, J.C.D. da Costa, Effect of nano-Al_2O_3 addition on the densification of YSZ electrolytes, Journal of Nano Research 6 (2009) 115–122.
[12] Ikesue Akio, A method to produce transparent YAG, Patent no JP 5294722, November 1993.
[13] K. Katayama, H. Õsawa, T. Akiba, K. Urabe, H. Yanagida, Sintering of yttrias with addition of divalent metal oxide and water vapour pressure dependence of their electrical conductivity, Journal of Materials Science 25 (1990) 1503–1508.
[14] Ide Takayuki, Kiyohara Masakatsu, Yttriia sintered body and corrosion-resistant material, and manufacturing method, US patent no. 2,007,161,499 (A1), August 2008.
[15] W.S. Young, I.B. Cutler, Initial sintering with constant rates of heating, Journal of the American Ceramic Society 53 (1970) 659–663.
[16] J. Wang, R. Raj, Estimate of the activation energies for boundary diffusion from rate-controlled sintering of pure alumina, and alumina doped with zirconia or titania, Journal of the American Ceramic Society 73 (1990) 1172–1175.
[17] K. Matsui, N. Ohmichi, M. Ohgai, N. Enomoto, J. Hojo, Sintering kinetics at constant rates of heating: effect of Al_2O_3 on the initial sintering stage of fine zirconia powder, Journal of the American Ceramic Society 88 (2005) 3346–3352.
[18] K. Matsui, A. Matsumoto, M. Uehara, N. Enomoto, J. Hojo, Sintering kinetics at isothermal shrinkage: effect of specific surface area on the initial sintering stage of fine zirconia powder, Journal of the American Ceramic Society 90 (2007) 44–49.
[19] D.L. Johnson, I.B. Cutler, Diffusion sintering: I, initial stage sintering models and their application to shrinkage of powder compacts, Journal of the American Ceramic Society 46 (1963) 541–545.
[20] Y. Moriyoshi, W. Komatsu, Kinetics of sintering at a constant rate of heating, Yogyo-Kyokai-Shi 79 (10) (1971) 370–375.
[21] X.-H. Wang, P.-L. Chen, I.W. Chen, Two-step sintering of ceramics with constant grain-size, I. Y_2O_3, Journal of the American Ceramic Society 89 (2006) 431–437.
[22] W.S. Colenz, J.M. Dynys, R.I. Coble, Initial stage solid state sintering models. A critical analysis and assessment, Materials Science Research 13 (1980) 141–157.
[23] D.L. Johnson, I.B. Cutler, Diffusion sintering: II, initial sintering kinetics of alumina, Journal of the American Ceramic Society 46 (1963) 545–550.
[24] C. Rüssel, A pyrolytic route to fluoride glasses. I. Preparation and thermal decomposition of metal trifluoroacetates, Journal of Non-Crystalline Solids 152 (1993) 161–166.
[25] M. Mosiadz, K.L. Juda, S.C. Hopkins, J. Soloducho, B.A. Glowacki, An in-depth in situ IR study of the thermal decomposition of copper trifluoroacetate hydrate, Journal of Fluorine Chemistry 135 (2012) 59–67.
[26] S. Kim, S. Ohtsuka, T. Kaito, S. Yamashita, M. Inoue, T. Asayama, T. Shobu, Formation of nano-size oxide particles and δ-ferrite at elevated temperature in 9Cr-ODS steel, Journal of Nuclear Materials 417 (2011) 209–212.
[27] A.J. Feighery, J.T.S. Irvine, D.P. Fagg, A. Kaiser, Phase relations at 1500 °C in the ternary system ZrO_2–Y_2O_3–TiO_2, Journal of Solid State Chemistry 143 (1999) 273–276.
[28] N. Mizutani, Y. Tajima, M. Kato, Phase relations in the systemY_2O_3–TiO_2, Journal of the American Ceramic Society 59 (1976) 168–169.
[29] M.L. In, A.M. Alper, B_2O_3–Y_2O_3 phase diagram, Phase Diagram 3 (1970) 180.
[30] J. Madarász, E. Beregi, J. Sztatisz, I. Földvári, G. Pokol, Combined DTA and XRD study of sintering steps towards $YAl_3(BO_3)_4$, Journal of Thermal Analysis and Calorimetry 64 (2001) 1059–1065.
[31] D. Boyer, G. Bertrand-Chadeyron, R. Mahiou, A. Brioude, J. Mugnier, Synthesis and characterization of sol–gel derived Y_3BO_6:Eu^{3+} powders and films, Optical Materials 24 (2003) 35–41.
[32] J.H. Lin, S. Zhou, L.Q. Yang, G.Q. Yao, M.Z. Su, L.P. You, Structure and luminescent properties of $Y_{17.33}(BO_3)_4(B_2O_5)_2O_{16}$, Journal of Solid State Chemistry 134 (1997) 158–163.
[33] S. Hosokawa, Y. Tanaka, S. Iwamoto, M. Inoue, Morphology and structure of rare earth borate ($REBO_3$) synthesized by glycothermal reaction, Journal of Materials Science 43 (2008) 2276–2285.
[34] H.G. Scott, Phase relationships in the zirconia–yttria system, Journal of Materials Science 10 (1975) 1527–1535.
[35] V.S. Stubican, J.R. Hellmann, Phase equilibrium in some zirconia systems, Advanced Ceramics 3 (1981) 25–36.
[36] V.S. Stubican, R.C. Hink, S.P. Ray, Phase equilibria and ordering in the system ZrO_2–Y_2O_3, Journal of the American Ceramic Society 61 (1978) 17–21.
[37] W.D. Tuohig, T.Y. Tien, Subsolidus phase equilibria in the system ZrO_2–Y_2O_3–Al_2O_3, Journal of the American Ceramic Society 63 (1980) 595–596.
[38] C. Brecher, G.C. Wei, W.H. Rhodes, Point defects in optical ceramics: high-temperature absorption processes in lanthana-strengthened yttria, Journal of the American Ceramic Society 73 (1990) 1473–1488.
[39] N. Rahaman, Ceramic Processing, CRC/Taylor & Francis Press, London, 2008.
[40] Y.H. Huang, D. Jiang, J. Zhang, Q. Lin, Fabrication of transparent lanthanum-doped yttria ceramics by combination of two-step sintering and vacuum sintering, Journal of the American Ceramic Society 92 (2009) 2883–2887.
[41] E. Lukin, N. Makarov, Sintering kinetics of aluminum oxide ceramics with an additive of eutectic composition, Glass and Ceramics 57 (2000) 23–25.
[42] S.C. Hu, L.C. De Jonghe, Pre-eutectic densification in MgF_2–CaF_2, Ceramics International 9 (1983) 123–126.
[43] S.J. Wu, L.C.D. Jonghe, M.N. Rahaman, Subcutectic densification and second-phase formation in Al_2O_3–CaO, Journal of the American Ceramic Society 68 (1985) 385–388.
[44] J. Luo, H. Wang, Y.-M. Chiang, Origin of solid-state activated sintering in Bi_2O_3-doped ZnO, Journal of the American Ceramic Society 82 (1999) 916–920.